COUPLING BETWEEN STRUCTURE AND LIQUID IN A PARALLEL-STAGE SPACE SHUTTLE DESIGN

D. D. Kana, W. L. Ko, P. H. Francis and A. Nagy

July 5, 1972

Backup Document for AIAA Synoptic Scheduled for Publication in Journal of Spacecraft and Rockets, November 1972

Southwest Research Institute
Department of Mechanical Sciences
8500 Culebra Road
San Antonio, Texas 78284

SYNOPTIC BACKUP DOCUMENT

This document is made publicly available through the NASA scientific and technical information system as a service to readers of the corresponding "Synoptic" which is scheduled for publication in the following (checked) technical journal of the American Institute of Aeronautics and Astronautics.

- ☐ AIAA Journal
- ☐ Journal of Aircraft
- ☒ Journal of Spacecraft & Rockets, Nov. 1972
- ☐ Journal of Hydronautics

A Synoptic is a brief journal article that presents the key results of an investigation in text, tabular, and graphical form. It is neither a long abstract nor a condensation of a full length paper, but is written by the authors with the specific purpose of presenting essential information in an easily assimilated manner. It is editorially and technically reviewed for publication just as is any manuscript submission. The author must, however, also submit a full backup paper to aid the editors and reviewers in their evaluation of the synoptic. The backup paper, which may be an original manuscript or a research report, is not required to conform to AIAA manuscript rules.

For the benefit of readers of the Synoptic who may wish to refer to this backup document, it is made available in this microfiche (or facsimile) form without editorial or makeup changes.

COUPLING BETWEEN STRUCTURE AND LIQUID PROPELLANTS IN A PARALLEL-STAGE SPACE SHUTTLE DESIGN*

D. D. Kana, W. L. Ko, P. H. Francis and A. Nagy
Southwest Research Institute
San Antonio, Texas

Abstract

A study was conducted to determine the influence of liquid propellants on the dynamic loads for space shuttle vehicles. A parallel-stage configuration model was designed and tested to determine the influence of liquid propellants on coupled natural modes. A forty degree-of-freedom analytical model was also developed for predicting these modes. Currently available analytical models were used to represent the liquid contributions, even though coupled longitudinal and lateral motions are present in such a complex structure. Agreement between the results was found in the lower few modes.

Nomenclature

a	distance between subsystems 2 and 11
$\underset{\sim}{a}$	coefficient matrix of constraint coordinates appearing in equations of motion
b	distance between subsystem 11 and the centerline of the Orbiter
c	distance between subsystems 12 and 13
$\underset{\sim}{c}$	constraint matrix
D_k	distance between the neutral axis of a rein forcing beam section and a cylinder shell ($k = 1, 2, 3, 4$)
d	distance between subsystems 15 and 16
$\underset{\sim}{d}$	coefficient matrix of mass coordinates appearing in equations of constraint
E_s	modulus of elasticity of cylinder shells ($s = 1, 2, 3, 5, 6, 7$)
$E^{(m)}$	modulus of elasticity of a reinforcing beam section ($m = 1, 2, 3, 4$)
e	distance between subsystem 5 and the rod $K^{(5)}$
F_i	$; (4/\pi)\, I_1(\mu_i)/\mu_i I_o(\mu_i)$ $\quad (i = 1, 3, 5, 7)$
G_s	shear modulus of cylinder shell s
g	gravitational constant
H	total number of dynamic and constraint equations of the mechanical system
h_i	height of liquid in cylinder i
$\tilde{h}_i$	height of horizontal sloshing mass in cylinder i
h_i^*	height of rigid mass in cylinder i
$\mathcal{I}_s$	moment of inertia of a cylinder cross section
I_o	modified Bessel function of order zero
I_1	modified Bessel function of order one
J_n	moment of inertia of mass element M_n ($n = 1, 2, \ldots, 8$)
$J^{(m)}$	moment of inertia of a reinforcing beam cross section
J_i^*	moment of inertia of rigid mass m_i^*
$J_{rigid}^{(i)}$	moment of inertia of frozen liquid in cylinder i
K_i	equivalent longitudinal spring constant of cylinder i accounting for liquid effect
K_j	longitudinal spring constant of cylinder j, ($j = 2, 6$); $2\pi R_j \delta_j E_j / \ell_j$
$\bar{K}_i$	longitudinal spring constant of cylinder i with liquid effect; $2\pi R_i \delta_i E_i / (\ell_i - \nu_i^2 h_i)$
$K^{(m)}$, $\bar{K}^{(3)}$, $\bar{K}^{(4)}$	longitudinal spring constants of the reinforcing beam sections
$K^{(6)}$, $K^{(7)}$	vertical and horizontal spring constants of the coupling spring system
k_i	vertical sloshing spring constant
$\bar{k}_i$	vertical sloshing spring constant due to Poisson's effect of the cylinder

* The results presented in this paper were obtained during the course of research sponsored by NASA Langley Research Center under Contract No. NAS1-9890.

This is a revision of AIAA Paper 72-347.

k_i' ; $\pi^2 \mu_i \delta_i E_i F_i / 2$

$\tilde{k}_i$ lateral sloshing spring constant

L number of dynamic equations

L' number of constraint equations

ℓ_s length of cylinder section

M_n structure mass element

$M_{( )}$, $\bar{M}_{( )}$ end moments of a beam section

$M_{[\ ]_{( )}}$,

$\bar{M}_{[\ ]_{( )}}$ net end moments of a shell-beam section

m_i vertical sloshing mass in cylinder i

$\tilde{m}_i$ horizontal sloshing mass in cylinder i

m_i^* rigid mass in cylinder i

$m_T^{(i)}$ total mass of the liquid in cylinder i; $\pi R_i^2 h_i \rho_i$

$P_{( )( )}$ mass matrix of the total system of dynamic and constraint equations

$\underset{\sim}{p}$ mass matrix of the dynamic equations only

$Q_{( )( )}$ stiffness matrix of the total system of dynamic and constraint equations

$\underset{\sim}{q}$ stiffness matrix of the dynamic equations only

R_s R_B (Booster radius) for s = 1, 2, 3; R_O (Orbiter radius) for s = 5, 6, 7

S_r torsional spring constant (r = 1, 2, . . . , 7)

t time

$V_{( )}$ lateral shearing force on an end cross section of a beam section

$V_{[\ ]_{( )}}$ net lateral shearing force on an end cross section of a shell-beam section

$W_{( )}$ vibration mode

$\underset{\sim}{X}$ coordinates associated with mass elements (see Table III)

$\underset{\sim}{x}$ coordinates associated with constraint conditions (see Table III)

$x_{( )}$ lateral displacement of a subsystem

$Y_{( )}$ amplitude of a vibration mode

$y_{( )}$ axis of rotation of a subsystem

$z_{( )}$ vertical displacement of a subsystem

$\alpha_{( )}$ rotation of a cross section of a shell beam where a horizontal sloshing spring or a rigid mass is attached

γ phase angle

δ_s cylinder shell thickness

$\zeta_{( )}$ vertical displacement of a vertical sloshing mass

$\eta_{( )}$ horizontal displacement of a lateral sloshing mass

μ_i liquid height parameter for cylinder i; $(\pi R_i / 2h_i)$

ν_s Poisson's ratio of cylinder shell

$\xi_{( )}$ horizontal displacement of a shell beam cross section where the lateral sloshing spring or a rigid mass is attached

ρ_i mass density of liquid in cylinder i

$\varphi_{( )}$ rotation of a structure subsystem

Ω eigenvalue of a vibration mode

ω frequency

Introduction

Currently specified design requirements of a space shuttle vehicle are anticipated to present many new problems heretofore not encountered in aerospace systems. The dynamic interaction between elastic structure and liquid propellants has always been an important design criteria for launch vehicles and aircraft; however, it is surmised that potential problems posed by this interaction will become even more critical in presently envisioned space shuttle systems[1]. Therefore, the purpose of this study is to examine the applicability of existing analytical techniques for studying the coupled liquid-structural dynamics of a typical space shuttle configuration—a parallel-stage design.

The program objective has been accomplished by developing a suitable experimental model that is capable of experiencing at least the most fundamental structural dynamics of a prototype system, measuring its natural frequencies of vibration for a range of various parameters, and comparing the results with those predicted from a corresponding analytically derived model. In selecting the model details from the outset, considerable effort was exercised to utilize components which were already available from previous research programs, in

order to minimize fabrication costs. Further, existing concepts of spring-mass fluid models, which have been derived to simulate liquid reactions for decoupled lateral and longitudinal motions, are employed in a straightforward manner in a system which experiences strong coupling along these axes. The results of this study of a rather fundamental model will point toward the path to follow for more complex representations of a shuttle system. We begin with a description of the physical model, then outline the analysis, and finally present results and conclusions from the study.

Description of Physical Model

A model consisting of a parallel-stage Booster and Orbiter, each consisting of two propellant tanks and appropriate intermediate skirts and rigid masses, was considered feasible to carry out the program objectives. The major portion of the Booster was already on hand from a previous study[2] of longitudinal dynamics in axisymmetrical launch vehicles. As a result, as will be seen, it also included some components, such as stiffeners and baffles, which were not strictly essential to the present study. Nevertheless, the presence of these extra components did not alter the conclusions of the study.

A photograph of the completely assembled and suspended system is shown in Fig. 1a, as it was used during most of the experiments. In order to provide a quick overall indication for model size and typical rigid masses, a schematic is shown in Fig. 1b. Further details will be given now, as well as in later sections of the report.

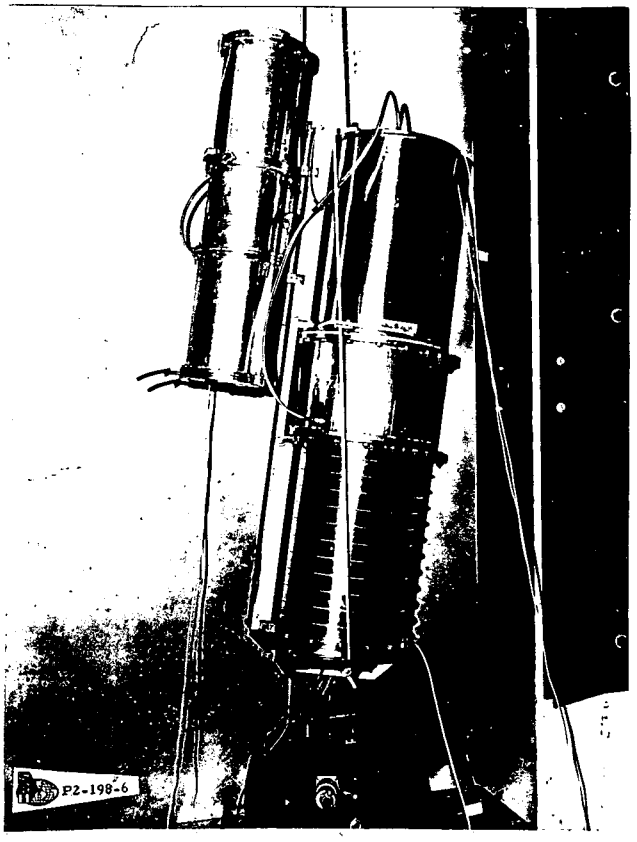

Fig. 1a. SwRI Space Shuttle Vehicle Dynamic Model

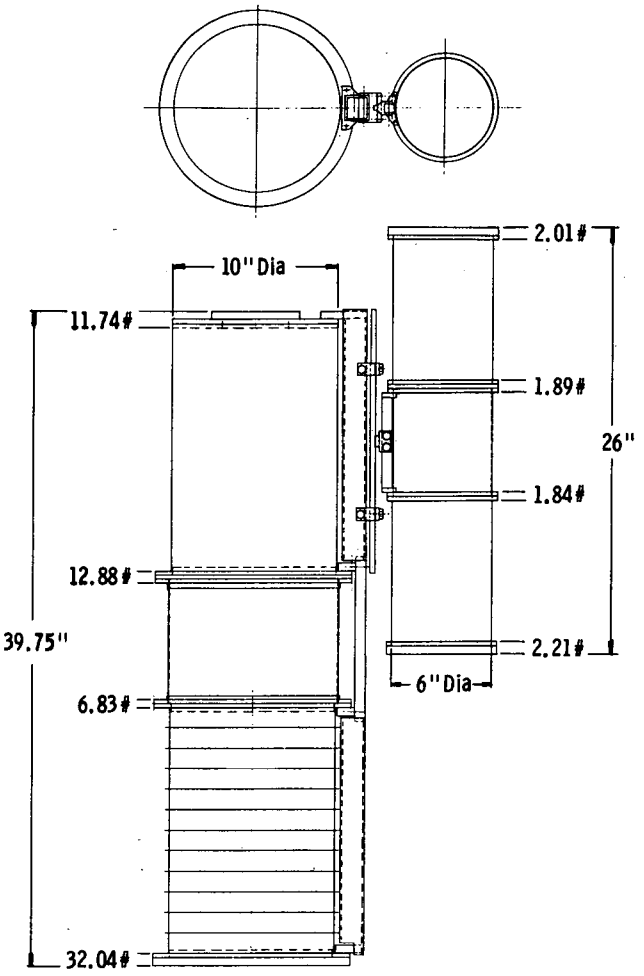

Fig. 1b. Schematic of Space Shuttle Vehicle Model

The Booster comprises the major part of the model, and it consists of the following main components:

(1) Upper tank
(2) Lower tank
(3) Skirt
(4) Bulkheads

Both tanks in the Booster model were fabricated from 0.005-in. thick, type 302 Stainless Steel sheets, which were rolled and butt-welded along longitudinal seams. A flat steel disk was spot-welded to one of the tanks which serves as a top mass for the upper tank. The lower end of this upper tank and both ends of the lower tank were spot-welded to identical steel flanges, which can be bolted to the bulkheads and the skirt as required. Two rows of spot welds, each spot weld

having a test strength of 25 pounds, were used at each end of the tanks. The spots were spaced 1/8-in. apart with 1/8-in. spacing between the rows. To provide for ullage pressure integrity, the ends of both tanks were sealed with epoxy cement.

The third main component in the Booster is the skirt. It was fabricated by rolling 0.025-in. thick, 6061-T6 aluminum sheet to the desired diameter and butt-welding it along a longitudinal seam. Two aluminum flanges were welded to the end of this cylinder with the same hole pattern as on the flanges of the tanks to provide for bolted assembly of these parts. Two small ports on the side of the skirt served as a pressure port for introducing ullage pressure to the lower tank and for filling the tank with liquid.

Flat, rigid bulkheads were machined from mild steel and 6061-T6 aluminum plates for the lower and upper tanks, respectively, with a shoulder on them so they could partially fit inside the tanks. The shoulders and their hole patterns match the flanges on the tanks. The lower ends of the tanks were sealed by these flat, rigid bulkheads by bolting them to the corresponding flanges. The tanks in turn were joined by bolting them together using the skirt as a coupling.

The lower tank had stiffener rings, stringers, and baffles installed on it. Eleven 6061-T6 aluminum rings, 0.032-in. thick were cemented on the outside of the tank 1.25 in. apart, symmetrically about midspan. Twelve 6061-T6 aluminum stringers, 1/8 x 1/8 x 14 in. in dimensions, were fastened to the inside of the tank by use of epoxy. The stringers were equally spaced around the circumference of the tank and symmetrical about midspan. Tapped holes along the length of these stringers provided the means for installing eleven yellow brass ring baffles into the tank. Data pertaining to the Booster model are given in Table I.

The Orbiter model, similar to the Booster, consists of two tanks with flat, rigid bulkheads and a skirt. The tanks and the skirt were fabricated from 0.012-in.-thick and 0.020-in.-thick 1100-H14 aluminum sheets, respectively, which were rolled and butt-welded along a longitudinal seam in the same manner as the Booster. Identical flanges with 16-hole bolt patterns were welded to each end of both tanks and skirt by a continuous weld.

Flat, rigid bulkheads were machined from 6061-T6 aluminum plates with hole patterns matching the pattern on the flanges. These bulkheads, however, did not have shoulders on them as was the case for the Booster. Plates identical to the bulkheads were used for capping both of the tanks on the Orbiter with provisions for introduction of ullage pressure and modeling liquid.

The skirt, as in the case of the Booster, was used to join the two tanks. Data pertaining to the Orbiter model are given in Table II.

Table I. Material Properties and Geometry of Structural Components of Booster Model

Structural Element	Effective Length(ℓ) (in.)	Inside Dia. (in.)	Wall Thickness (in.)	Material Density (#/in^3)	E $\times 10^6$ psi
Upper Tank	14.5	10.0	0.005	0.29	29
Lower Tank	14.5	10.0	0.005	0.29	29
Skirt	7.5	10.3	0.025	0.098	10

	Material Density (#/in^3)	E $\times 10^6$ psi	Dimensions (in.)
Flat Rigid Bulkhead Lower Tank	0.29	30	9.875 Dia., 1/2 Height, 12 Dia. shoulder, 1/2 Height
Flat Rigid Bulkhead Upper Tank	0.098	10	9.875 Dia., 1/2 Height, 12 Dia. shoulder, 1/2 Height

	Number Used on Tank	Material Density (#/in^3)	E $\times 10^6$ psi	Dimensions (in.)	Location	Spacing (in.)
Stiffener Ring	11	0.098	10	10.0 I.D. 10.5 O.D. 0.032 thick	Symmetrical about midspan	1.24
Stringer	12	0.098	10	0.125 X 0.125 X 14.0	Symmetrical about midspan	Equally spaced on inner circumference
Baffle	11	0.306	16	0.25 I.D. 9.68 O.D. 0.0125 thick	Symmetrical about midspan	1.25

Table II. Material Properties and Geometry of Structural Components of Orbiter Model

Structural Element	Effective Length(ℓ) (in.)	Inside Dia. (in.)	Wall Thickness (in.)	Material Density (#/in^3)	E $\times 10^6$ psi
Upper Tank	8.5	6.0	0.012	0.098	10
Lower Tank	8.5	6.0	0.012	0.098	10
Skirt	6.0	6.0	0.020	0.098	10

	Diameter (in.)	Thickness (in.)	Material Density (#/in^3)	E $\times 10^6$ psi
Bulkheads	6.7	0.25	0.098	10
Caps	6.7	0.25	0.098	10

Coupling between the Booster and Orbiter was achieved by the strongback assembly. As can be seen in Fig. 1, the strongback spans the full length of the Booster and is attached to it at four locations, namely, at each flange and the top. This part of the strongback was fabricated from a $1\frac{1}{2} \times 1\frac{1}{2} \times \frac{1}{8}$-in., 6063-T5 aluminum square tube with appropriate altering to be attachable to the Booster.

A short backstrap was attached to the Orbiter spanning between the two flanges of the skirt. To this backstrap, a 1/4-in. square steel rod was fastened which fits into two guides on the strongback allowing adjustment of the relative position between the Booster and Orbiter.

Analytical Model

Mechanical Model

In the modal analysis of free vibration of the model Shuttle Vehicle, the system is represented by the equivalent mechanical model shown in Fig. 2a. The motion of the system will be limited to translations in x and z directions and pitching about an axis perpendicular to xz plane. The cylindrical shells between any two neighboring mass elements will be represented by thin-walled beam-like tubes, or shell-beams, as shown in Fig. 2b. Additional details are given in Figs. 2c and 2d. Masses of the cylindrical shell sections, Booster and Orbiter strongback beam sections, and between any two neighboring mass elements are divided equally into two parts, each of which is lumped into each of the two mass elements. Thus, the inertia effect of the shells and the strongback beams will be otherwise neglected. The Booster and the Orbiter strongback reinforcing beams are pin-jointed, respectively, to the Booster and the Orbiter mass elements with one torsional spring attached to each joint. The two beams are then connected together through a coupling compound spring system which permits relative displacements in x and z directions, and one relative rotation about an axis perpendicular to the xz plane. The lower end of the Orbiter is connected to the Booster strongback beam through a rod $K^{(5)}$ both of whose ends are pin-jointed. *

The vertical and lateral sloshing motions of the liquid in a cylinder are represented independently by two sloshing models. The vertical sloshing model[3] consists of one vertical sloshing mass $m_i (i = 1, 3, 5, 7)$ connected to the neighboring mass elements through two springs** k_i and $\bar{k}_i$. It will be assumed that the bending of the shell-beam does not interfere with the motion of m_i. The lateral sloshing model† [4, 5, 6] consists of one rigid mass m_i^* rigidly attached to the shell-beam, and one lateral sloshing mass $\tilde{m}_i$ connected to the shell-beam through two springs of spring constant $\tilde{k}_i/2$. For the vertical sloshing, quantities associated with the horizontal sloshing (i.e., m_i^*, $\tilde{m}_i$, and $\tilde{k}_i$) will be set to zero, and vice versa.

The vertical sloshing mass m_i and the sloshing spring constants k_i and $\bar{k}_i$ are defined as follows[3]

$$m_i = 4F_i m_T^{(i)}; \quad (i = 1, 3, 5, 7) \tag{1}$$

$$k_i = k_i' - \nu_i \bar{K}_i F_i + \nu_i^2 \bar{K}_i F_i^2; \quad \text{(no summation)} \tag{2}$$

$$\bar{k}_i = \nu_i \bar{K}_i F_i \tag{3}$$

The lateral sloshing mass for the first mode or fundamental slosh mass $\tilde{m}_i$, and its height $\tilde{h}_i$, the rigid mass m_i^* and its height h_i^* and the sloshing spring constant are defined in the following[4, 5, 6]

$$\tilde{m}_i = m_T^{(i)} \left(\frac{R_i}{2.2 h_i} \right) \tanh 1.84 \frac{h_i}{R_i} \tag{4}$$

$$m_i^* = m_T^{(i)} - \tilde{m}_i \tag{5}$$

$$\tilde{k}_i = m_T^{(i)} \left(\frac{g}{1.19 h_i} \right) \left(\tanh 1.84 \frac{h_i}{R_i} \right)^2 \tag{6}$$

$$\tilde{h}_i = h_i - \frac{R_i}{0.92} \tanh 0.92 \frac{h_i}{R_i}$$

$$= \text{height of } \tilde{m}_i \tag{7}$$

$$h_i^* = h_i - \frac{m_T^{(i)} h_i}{2 m_i^*} + (h_i - \tilde{h}_i) \frac{\tilde{m}_i}{m_i^*}$$

$$= \text{the height of } m_i^* \tag{8}$$

The polar moment of inertia of m_i^* is defined as

$$J_i^* = J_{\text{rigid}}^{(i)} + m_T^{(i)} \frac{h_i^2}{4} - \frac{m_T^{(i)} R_i^2}{2} \times \left[1.995 - \frac{2.14 R_i}{h_i} \tanh 0.92 \frac{h_i}{R_i} \right] - m_i^* (h_i - h_i^*)^2 - \tilde{m}_i (h_i - \tilde{h}_i)^2 \tag{9}$$

where

$$J_{\text{rigid}} = \frac{m_T^{(i)} R_i^2}{4} \left[\frac{1}{3} \frac{h_i^2}{R_i^2} + 1 \right] \tag{10}$$

Figures 2a and 2b show that $\tilde{m}_i$ is situated above m_i^*; however, as the depth of the liquid h_i decreases, $\tilde{m}_i$ will shift to a position below m_i^*.

Mathematical Formulation

The free dynamic behavior of the mechanical model can be described completely in mathematical terms by writing the equations of motion and equations of constraint for the system. In order to do this, the mechanical model is divided into subsystems for which equations of dynamic and static equilibrium for the free oscillation can easily be set up. The coordinate system at each subsystem is shown in Fig. 2a.

In the model, the structure mass elements $M_n (n = 1, 2, \ldots, 8)$ will have three degrees of freedom in motion (two translations and one rotation), the rigid mass $m_i^* (i = 1, 3, 5, 7)$ two degrees of freedom (one horizontal translation and one

*This rod was removed from the experimental apparatus and, consequently, its effect was nullified in the numerical program by setting to zero its cross-sectional area.

**All springs in the model are massless and linear.

†This model was originally developed for a rigid container.

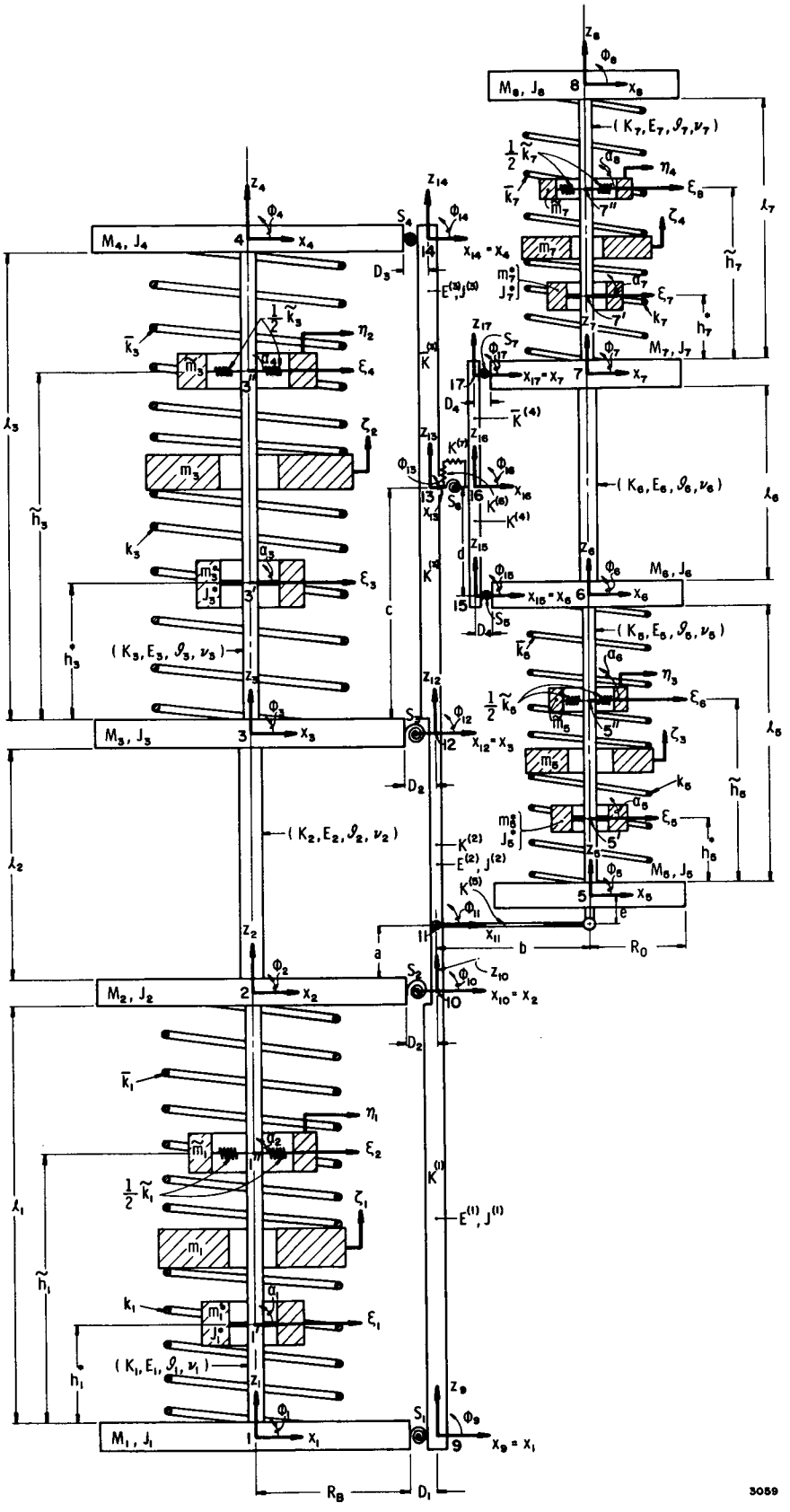

Fig. 2a. Equivalent Mechanical Model

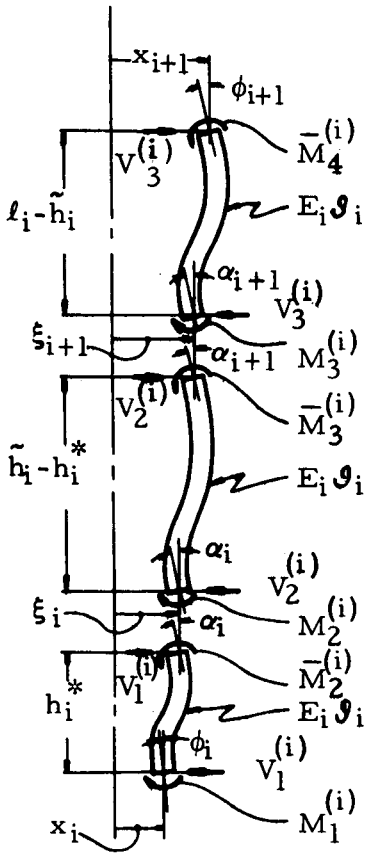

$$\bar{M}_4^{(i)} = \frac{2E_i\vartheta_i}{N_{i3}(\ell_i-\tilde{h}_i)^2}\left[3(x_{i+1}-\xi_{i+1}) + (\ell_i-\tilde{h}_i)(2\phi_{i+1}A_{i3}+\alpha_{i+1}B_{i3})\right]$$

$$V_3^{(i)} = \frac{6E_i\vartheta_i}{N_{i3}(\ell_i-\tilde{h}_i)^3}\left[2(x_{i+1}-\xi_{i+1}) + (\ell_i-\tilde{h}_i)(\alpha_{i+1}+\phi_{i+1})\right]$$

$$M_3^{(i)} = \frac{-2E_i\vartheta_i}{N_{i3}(\ell_i-\tilde{h}_i)^2}\left[3(x_{i+1}-\xi_{i+1}) + (\ell_i-\tilde{h}_i)(2\alpha_{i+1}A_{i3}+\phi_{i+1}B_{i3})\right]$$

$$\bar{M}_3^{(i)} = \frac{2E_i\vartheta_i}{N_{i2}(\tilde{h}_i-h_i^*)^2}\left[3(\xi_{i+1}-\xi_i) + (\tilde{h}_i-h_i^*)(2\alpha_{i+1}A_{i2}+\alpha_iB_{i2})\right]$$

$$V_2^{(i)} = \frac{6E_i\vartheta_i}{N_{i2}(\tilde{h}_i-h_i^*)^3}\left[2(\xi_{i+1}-\xi_i) + (\tilde{h}_i-h_i^*)(\alpha_i+\alpha_{i+1})\right]$$

$$M_2^{(i)} = \frac{-2E_i\vartheta_i}{N_{i2}(\tilde{h}_i-h_i^*)^2}\left[3(\xi_{i+1}-\xi_i) + (\tilde{h}_i-h_i^*)(2\alpha_iA_{i2}+\alpha_{i+1}B_{i2})\right]$$

$$\bar{M}_2^{(i)} = \frac{2E_i\vartheta_i}{N_{i1}(h_i^*)^2}\left[3(\xi_i-x_i) + h_i^*(2\alpha_iA_{i1}+\phi_iB_{i1})\right]$$

$$V_1^{(i)} = \frac{6E_i\vartheta_i}{N_{i1}(h_i^*)^3}\left[2(\xi_i-x_i) + h_i^*(\alpha_i+\phi_i)\right]$$

$$M_1^{(i)} = \frac{-2E_i\vartheta_i}{N_{i1}(h_i^*)^2}\left[3(\xi_i-x_i) + h_i^*(2\phi_iA_{i1}+\alpha_iB_{i1})\right]$$

Fig. 2b. Detail of i-th Shell Beam

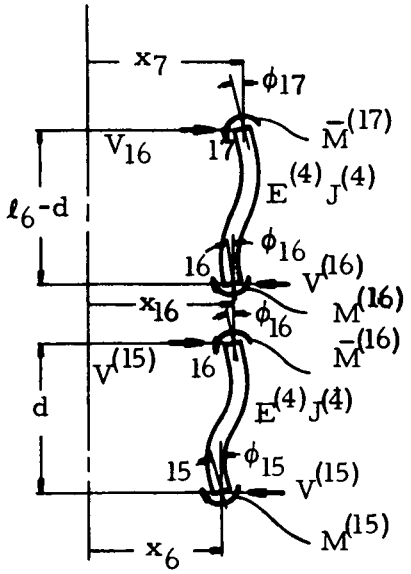

$$\bar{M}^{(17)} = \frac{2E^{(4)}J^{(4)}}{(\ell_6-d)^2}\left[3(x_7-x_{16}) + (\ell_6-d)(2\phi_{17}+\phi_{16})\right]$$

$$V^{(16)} = \frac{6E^{(4)}J^{(4)}}{(\ell_6-d)^3}\left[2(x_7-x_{16}) + (\ell_6-d)(\phi_{16}+\phi_{17})\right]$$

$$M^{(16)} = \frac{-2E^{(4)}J^{(4)}}{(\ell_6-d)^2}\left[3(x_7-x_{16}) + (\ell_6-d)(2\phi_{16}+\phi_{17})\right]$$

$$\bar{M}^{(16)} = \frac{2E^{(4)}J^{(4)}}{d^2}\left[3(x_{16}-x_6) + d(2\phi_{16}+\phi_{15})\right]$$

$$V^{(15)} = \frac{6E^{(4)}J^{(4)}}{d^3}\left[2(x_{16}-x_6) + d(\phi_{15}+\phi_{16})\right]$$

$$M^{(15)} = \frac{-2E^{(4)}J^{(4)}}{d^2}\left[3(x_{16}-x_6) + d(2\phi_{15}+\phi_{16})\right]$$

Fig. 2c. Detail of Orbiter Reinforcing Beam

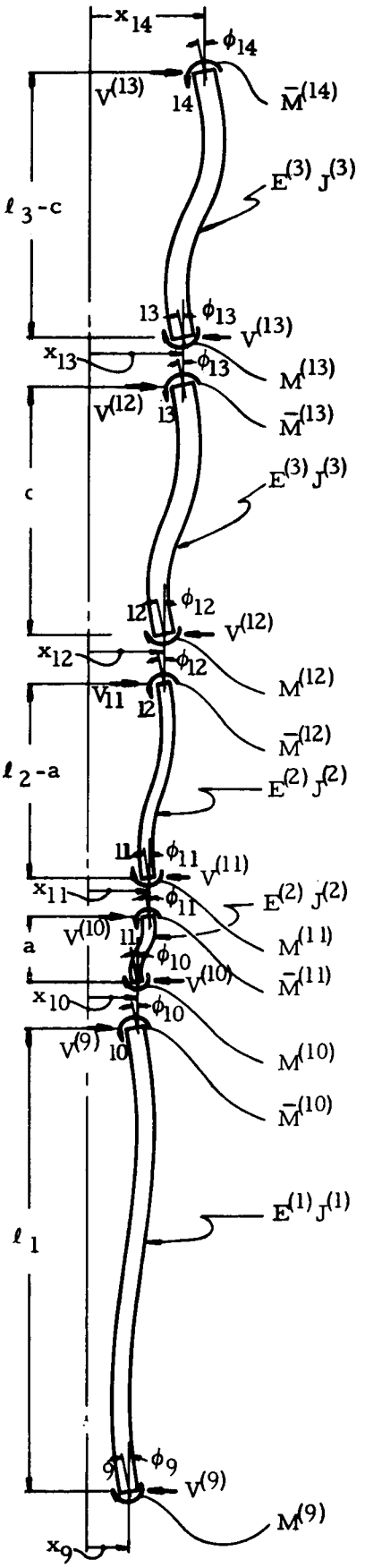

$$\bar{M}^{(14)} = \frac{2E^{(3)}J^{(3)}}{(\ell_3-c)^2}\left[3(x_4-x_{13})+(\ell_3-c)(2\phi_{14}+\phi_{13})\right]$$

$$V^{(13)} = \frac{6E^{(3)}J^{(3)}}{(\ell_3-c)^3}\left[2(x_4-x_{13})+(\ell_3-c)(\phi_{13}+\phi_{14})\right]$$

$$M^{(13)} = \frac{-2E^{(3)}J^{(3)}}{(\ell_3-c)^2}\left[3(x_4-x_{13})+(\ell_3-c)(2\phi_{13}+\phi_{14})\right]$$

$$\bar{M}^{(13)} = \frac{2E^{(3)}J^{(3)}}{c^2}\left[3(x_{13}-x_3)+c(2\phi_{13}+\phi_{12})\right]$$

$$V^{(12)} = \frac{6E^{(3)}J^{(3)}}{c^3}\left[2(x_{13}-x_3)+c(\phi_{12}+\phi_{13})\right]$$

$$M^{(12)} = \frac{-2E^{(3)}J^{(3)}}{c^2}\left[3(x_{13}-x_3)+c(2\phi_{12}+\phi_{13})\right]$$

$$\bar{M}^{(12)} = \frac{2E^{(2)}J^{(2)}}{(\ell_2-a)^2}\left[3(x_3-x_{11})+(\ell_2-a)(2\phi_{12}+\phi_{11})\right]$$

$$V^{(11)} = \frac{6E^{(2)}J^{(2)}}{(\ell_2-a)^3}\left[2(x_3-x_{11})+(\ell_2-a)(\phi_{11}+\phi_{12})\right]$$

$$M^{(11)} = \frac{-2E^{(2)}J^{(2)}}{(\ell_2-a)^2}\left[3(x_3-x_{11})+(\ell_2-a)(2\phi_{11}+\phi_{12})\right]$$

$$\bar{M}^{(11)} = \frac{2E^{(2)}J^{(2)}}{a^2}\left[3(x_{11}-x_2)+a(2\phi_{11}+\phi_{10})\right]$$

$$V^{(10)} = \frac{6E^{(2)}J^{(2)}}{a^3}\left[2(x_{11}-x_2)+a(\phi_{10}+\phi_{11})\right]$$

$$M^{(10)} = \frac{-2E^{(2)}J^{(2)}}{a^2}\left[3(x_{11}-x_2)+a(\phi_{11}+2\phi_{10})\right]$$

$$\bar{M}^{(10)} = \frac{2E^{(1)}J^{(1)}}{\ell_1^2}\left[3(x_2-x_1)+\ell_1(2\phi_{10}+\phi_9)\right]$$

$$V^{(9)} = \frac{6E^{(1)}J^{(1)}}{\ell_1^3}\left[2(x_2-x_1)+\ell_1(\phi_9+\phi_{10})\right]$$

$$M^{(9)} = \frac{-2E^{(1)}J^{(1)}}{\ell_1^2}\left[3(x_2-x_1)+\ell_1(\phi_{10}+2\phi_9)\right]$$

Fig. 2d. Detail of Booster Reinforcing Beam

rotation), the lateral sloshing mass $\tilde{m}_i$ one degree of freedom (horizontal translation), and the vertical sloshing mass m_i one degree of freedom (vertical translation). Thus, the entire system will have forty degrees of freedom and therefore forty equations of motion. However, only equations associated with subsystem 1 will be shown for the purpose of illustration.

Equations of motion. At subsystem 1 there are two equations of motion for translation and one for rotation. They are

$$M_1\ddot{x}_1 - V_1^{(1)} - V^{(9)} = 0 \tag{11}$$

$$M_1\ddot{z}_1 - K^{(1)}\left[(z_2 - z_1) + (R_B+D_1)(\varphi_2-\varphi_1)\right] - K_1(z_2-z_1) - k_1(\zeta_1-z_1) = 0 \tag{12}$$

$$J_1\ddot{\varphi}_1 - K^{(1)}(R_B + D_1) \times \left[(z_2-z_1) + (R_B+D_1)(\varphi_2-\varphi_1)\right] + S_1(\varphi_1-\varphi_9) - M^{(1)} = 0 \tag{13}$$

where

D_1 = distance between the neutral axis of the Booster strongback beam section 9-10 and the Booster shell

K_1 = longitudinal spring constant of cylinder 1

$K^{(1)}$ = longitudinal spring constant of beam section 9-10

J_1 = polar moment of inertia of mass M_1 about y_1 axis

S_1 = torsional spring constant at joint 9

$$M_1^{(1)} = -\frac{2E_1\vartheta_1}{(h_1^*)^2N_{11}}\left[3(\xi_1 - x_1) + h_1^*(2A_{11}\varphi_1 + B_{11}\alpha_1)\right] \tag{14}$$

= net moment at lower end of shell-beam 1

$$V^{(9)} = \frac{6E^{(1)}J^{(1)}}{\ell_1^3}\left[2(x_2-x_1) + \ell_1(\varphi_9+\varphi_{10})\right] \tag{15}$$

= end shearing force of the Booster reinforcing beam section at end 9[7]

$$V_1^{(1)} = \frac{6E_1\vartheta_1}{(h_1^*)^3N_{11}}\left[2(\xi_1-x_1) + h_1^*(\varphi_1+\alpha_1)\right] \tag{16}$$

= net shearing force at lower end of shell-beam 1

$E^{(1)}$ = Young's modulus of the reinforcing beam section 9-10

$J^{(1)}$ = moment of inertia of the cross section of the reinforcing beam section 9-10

ϑ_1 = moment of inertia of the cylinder cross section

and

$$N_{11} = 1 + \frac{12E_1\vartheta_1}{(h_1^*)^2\pi R_B\delta_1G_1},$$

$$A_{11} = 1 + \frac{3E_1\vartheta_1}{(h_1^*)^2\pi R_B\delta_1G_1},$$

$$B_{11} = 1 - \frac{6E_1\vartheta_1}{(h_1^*)^2\pi R_B\delta_1G_1} \tag{17}$$

Equations (17) provide correction factors which arise from the analysis based on linear membrane theory of the shell. These factors are unity for an ordinary beam (see Ref. 8). Similar equations of motion may be written for the rest of subsystems.

Equations of constraint. As shown in Fig. 2a, at each massless subsystem of 9, 10, 12, 14, 15, and 17 there will be one constraint condition in the φ direction; at subsystem 11 there are two constraint conditions (x and φ directions); at subsystems 13 and 16 there are three constraint conditions (x, z, φ directions) for each subsystem; at subsystem i (i = 1, 3, 5, 7) there are two constraint conditions (α, ξ directions). Thus there will be twenty-two constraint conditions associated with the model. For the purpose of illustration only the constraint conditions at the massless subsystem 9 will be shown below.

$$0 \times \ddot{\varphi}_9 - S_1(\varphi_1-\varphi_9) - M^{(9)} = 0$$

where

$$M^{(9)} = -2E^{(1)}J^{(1)}\left[3(x_2-x_1) + \ell_1(2\varphi_9+\varphi_{10})\right]/\ell_1^2 \tag{18}$$

= end moment of the Booster reinforcing beam section at end 9

Similar constraint equations may be written for the rest of massless nodes.

Eigenvalue problem. Since only free oscillations are being considered, the aforementioned system of H equations of motion and constraint is homogeneous. Taken together, the total system of dynamic and constraint equations can be written in compact notation (employing the summation convention) as

$$P_{rs}\ddot{W}_s + Q_{rs}W_s = 0 \qquad r, s = 1, 2, \ldots, H \tag{19}$$

It is assumed that the vibration modes are harmonic, i.e.,

$$W_s = Y_s \cos(\omega t + \gamma) \tag{20}$$

where each frequency ω is real. On substituting Eq. (20) into Eq. (19), one finds

$$(Q_{rs} - \omega^2 P_{rs})(Y_s) = 0 \tag{21}$$

There is a well-known principle[7] in vibration theory which states that a system of H equations consisting of L dynamic and L′ constraint equations (L + L′ = H) can always be reduced to a problem involving L equations. This can be accomplished by incorporating the constraint equations into the equations of motion. In the present problem, this can be done by segregating the set of generalized coordinates $\underset{\sim}{W}$ into two nonintersecting sets:

$$\underset{\sim}{W} = \underset{\sim}{X} \cup \underset{\sim}{x}$$

where

$\underset{\sim}{X}$ = set of coordinates associated with mass elements

$\underset{\sim}{x}$ = set of coordinates associated with constraint conditions

For the present problem, $\underset{\sim}{X}$ and $\underset{\sim}{x}$ are defined in Table III. Equations (21) can now be replaced by two sets of equations, the first of which gives the L equations of motion expressed in terms of the constraint coordinates $\underset{\sim}{x}$:

$$(q_{ij} - \Omega^2 p_{ij})(X_j) = -a_{in} x_n$$

$$i, j = 1, 2, \ldots, L \qquad n = 1, 2, \ldots, L' \tag{22}$$

The second set of conditions relates the $\underset{\sim}{x}$ coordinates to the $\underset{\sim}{X}$ coordinates:

$$c_{lm} x_m = d_{lj} X_j \qquad l, m = 1, 2, \ldots, L' \tag{23}$$

This system of equations can be written such that the square matrix $\underset{\sim}{c}$ is symmetric and that $\underset{\sim}{d} = -\underset{\sim}{a}^T$. Solving for $\underset{\sim}{x}$:

$$x_n = c_{nl}^{-1} d_{lj} X_j \tag{24}$$

and substituting into Eq. (22):

$$(q_{ij} - \Omega^2 p_{ij})(X_j) = -a_{in} c_{nl}^{-1} d_{lj} X_j$$

$$= a_{in} c_{nl}^{-1} a_{lj}^T X_j \tag{25}$$

Thus:

$$\left[(q_{ij} - a_{in} c_{nl}^{-1} a_{lj}^T) - \Omega^2 p_{ij}\right](X_j) = 0 \tag{26}$$

By premultiplying by p^{-1} this equation takes the form of a standard eigenvalue problem

$$\left[p_{ki}^{-1}(q_{ij} - a_{in} c_{nl}^{-1} a_{lj}^T) - \Omega^2 \delta_{kj}\right](X_j) = 0,$$

$$k = 1, 2, \ldots, L \tag{27}$$

Nontrivial solutions for the eigenvector $\underset{\sim}{X}$ exist if, and only if, the determinant of the coefficient matrix vanishes:

$$\left| p_{ki}^{-1}(q_{ij} - a_{in} c_{nl}^{-1} a_{lj}^T) - \Omega^2 \delta_{kj} \right| = 0 \tag{28}$$

Thus, the problem reduces to finding the eigenvalues of the L × L matrix $\underset{\sim}{p}^{-1}(\underset{\sim}{q} - \underset{\sim}{a}\underset{\sim}{c}^{-1}\underset{\sim}{a}^T)$. The eigenvalues found by this process are the natural frequencies of the Booster/Orbiter system, expressed in radians/second. Included in this set of frequencies are the zero frequencies identified with translation and rotation of the system as a rigid body.

Table III. Definition of Coordinates

Coordinates Associated with Mass Elements		Coordinates Associated with Constraint Conditions	
$X_1 = z_1$	$X_{21} = x_5$	$x_1 = z_{13}$	$x_{12} = x_{11}$
$X_2 = z_2$	$X_{22} = x_6$	$x_2 = z_{16}$	$x_{13} = x_{13}$
$X_3 = z_3$	$X_{23} = x_7$	$x_3 = \phi_9$	$x_{14} = x_{16}$
$X_4 = z_4$	$X_{24} = x_8$	$x_4 = \phi_{10}$	$x_{15} = \alpha_6$
$X_5 = z_5$	$X_{25} = \zeta_3$	$x_5 = \phi_{11}$	$x_{16} = \alpha_8$
$X_6 = z_6$	$X_{26} = \zeta_4$	$x_6 = \phi_{12}$	$x_{17} = \xi_6$
$X_7 = z_7$	$X_{27} = \alpha_5$	$x_7 = \phi_{13}$	$x_{18} = \xi_8$
$X_8 = z_8$	$X_{28} = \alpha_7$	$x_8 = \phi_{14}$	$x_{19} = \alpha_2$
$X_9 = \phi_1$	$X_{29} = \xi_5$	$x_9 = \phi_{15}$	$x_{20} = \alpha_4$
$X_{10} = \phi_2$	$X_{30} = \xi_7$	$x_{10} = \phi_{16}$	$x_{21} = \xi_2$
$X_{11} = \phi_3$	$X_{31} = \eta_3$	$x_{11} = \phi_{17}$	$x_{22} = \xi_4$
$X_{12} = \phi_4$	$X_{32} = \eta_4$		
$X_{13} = \phi_5$	$X_{33} = \zeta_1$		
$X_{14} = \phi_6$	$X_{34} = \zeta_2$		
$X_{15} = \phi_7$	$X_{35} = \alpha_1$		
$X_{16} = \phi_8$	$X_{36} = \alpha_3$		
$X_{17} = x_1$	$X_{37} = \xi_1$		
$X_{18} = x_2$	$X_{38} = \xi_3$		
$X_{19} = x_3$	$X_{39} = \eta_1$		
$X_{20} = x_4$	$X_{40} = \eta_2$		

In the present problem, the matrix $\underset{\sim}{q}$ and the matrix $\underset{\sim}{a}\underset{\sim}{c}^{-1}\underset{\sim}{a}^T$ both are symmetric, and the matrix $\underset{\sim}{p}$ is diagonal (and, hence, $\underset{\sim}{p}^{-1}$ is diagonal). However, the product matrix $\underset{\sim}{p}^{-1}(\underset{\sim}{q} - \underset{\sim}{a}\underset{\sim}{c}^{-1}\underset{\sim}{a}^T)$ is not symmetric. Mathematically, the eigenvalues of a real, nonsymmetric matrix may be complex, all or in part. On physical grounds, however, one knows that the mathematical model being solved represents a linear conservative system, and therefore a correct solution must result in real eigenvalues. Complex eigenvalues introduce growth and decay characteristics in the modal

response which are inadmissible for the free vibrations of the problem under consideration. In the numerical solution for the present problem an eigenvalue routine was used which computes the complex eigenvalues of a nonsymmetric matrix. All nontrivial eigenvalues, however, were found to be real.

The nonzero elements of the matrices $\underset{\sim}{q}$, $\underset{\sim}{a}$, and $\underset{\sim}{c}$ are tabulated in Ref. 9 for three different cases: $\tilde{h}_i > h_i^*$, $\tilde{h}_i < h_i^*$ and the empty case.

Numerical Aspects

The physical quantities which are involved in the equations of motion and constraint for the analytical model consist of parameters which can be computed directly (masses, moments of inertia, etc.) and of terms which do not lend themselves to direct computation (effective* spring constants). These latter terms can be estimated from force-displacement calculations based on idealized models, but these estimates by no means serve as valid input data for computational purposes. Effective spring constants, in some cases, also can be determined experimentally by impedance techniques. The general approach used in this program for determining the input parameters for the analytical models was first to calculate by some means (quite approximately in some cases) all of the input data required of the model. Following this, certain of the parameters, least amenable to accurate calculation, were adjusted within certain narrow bounds in an attempt to match the frequencies computed theoretically with the experimental values for the empty tank case. This procedure is not the same as "curve fitting" where one takes much greater liberty with the number of parameters varied and disregards theoretical estimates on their magnitudes. The approach adopted here limits the amount of empiricism to a practical minimum in fixing the input data.

In the case of the Booster K_1 and K_2, the effective axial spring constants of the thin-walled shells were found experimentally by an axial vibration test, as described in the next section. The axial spring constants characterizing the strongback were adjusted from their calculated values to match the empty, decoupled booster data. For the Orbiter, the axial spring constant of cylinder 5 was calculated, and a correction factor (a corrected shell thickness δ_5) introduced to force agreement with the experimental result for cylinder 5 alone in both axial and bending motion. This procedure was repeated using cylinders 5 and 6 together, to determine K_6. For cylinder 7, δ_7 was taken equal to δ_5. The parameters finally arrived at are listed. Once so determined, they were held constant throughout all computational work.

K_1	=	3.48×10^5	lb/in.
K_2	=	7.36×10^5	lb/in.
$K^{(1)}$	=	1.8333×10^5	lb/in.
$K^{(2)}$	=	5.3571×10^5	lb/in.
$K^{(3)}$	=	3.4921×10^5	lb/in.
$K^{(4)}$	=	1.2083×10^6	lb/in.
$\bar{K}^{(3)}$	=	3.8596×10^5	lb/in.
$\bar{K}^{(4)}$	=	1.2083×10^6	lb/in.
δ_5	=	$\delta_7 = 9.84 \times 10^{-3}$	in.
K_6	=	1.885×10^5	lb/in.
S_5	=	$S_7 = 2.60 \times 10^4$	in.-lb/rad

In the case of the coupled Booster/Orbiter system three additional spring constants were available for adjustment, within limits, to match the theoretical and experimental coupled empty tank condition. These three constants represented the torsional coupling spring S_6, the vertical coupling spring $K^{(6)}$, and the horizontal coupling spring $K^{(7)}$. All three of these spring constants were first calculated on the basis of idealized models, to serve as nominal values in the adjustment process. The values finally chosen were:

S_6	=	3.9027×10^4	in.-lb/rad
$K^{(6)}$	=	2.677×10^5	lb/in.
$K^{(7)}$	=	9.9672×10^3	lb/in.

The calculations for the empty-tank condition omit the slosh models from the system of equations, and do not represent simply a degenerate case of vanishingly small liquid levels. The general system of equations, which does include the sloshing models, must predict frequencies compatible with the empty-tank results for small, but nonzero liquid levels. This criterion serves as a checkpoint on the accuracy of the numerical program. Also, a transition point occurs at a liquid level of 1.043 times the tank diameter, below which h_i^*, the location of the rigid mass, reverses its relative position with $\tilde{h}_i$, the location of the sloshing mass. On either side of this transition certain equations must be rewritten in a different form, with the result that the program differs according to whether one is considering a "near full" or a "near empty" tank. Continuity in the computed frequencies, of course, must be maintained across this transition point, and this criterion serves as an additional check on the programming accuracy.

*Note that effective spring constants include effects difficult to predict, such as bolted joint compliances and longitudinal stiffeners.

The matrix eigenvalue problem was solved on a CDC-6400 computer using a standard eigenvalue routine (modified Jacobi method) for finding the eigenvalues of a real, nonsymmetric matrix.

Experimental Procedure

The test program performed on the previously described physical model can be divided into distinctive phases and may be listed as the determination of:

(1) Effective spring constants for subassemblies

(2) Natural bending frequencies of decoupled Booster and Orbiter models

(3) Natural longitudinal frequencies of decoupled Booster and Orbiter modes

(4) Natural frequencies of Shuttle Vehicle Model.

The first part of the experimental program was to determine the effective spring constants of the Booster model components. This was accomplished by mounting the intermediate empty configurations illustrated in Fig. 3 on an electrodynamic shaker and determining the natural frequencies of the components. Frequencies obtained by this test were used to calculate the effective spring constants. Similar procedure was used with the Orbiter model components, both for axial and lateral excitation. The resulting spring constants were tabulated in the previous section for both models.

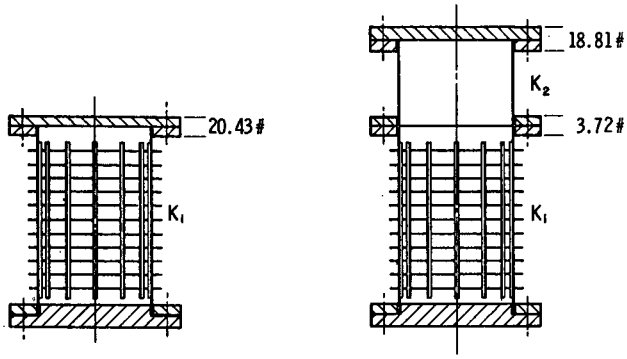

Fig. 3. Intermediate Empty Configuration of Booster Model

The second phase of the test program was devoted to determining the natural bending frequencies of the decoupled models. The Booster model was vertically suspended by a nylon rope, pulley, and spring combination which was designed to simulate a free-free condition. The rope was attached to the model at its bottom flange on the lower tank and was guided at the top of the skirt. A small electrodynamic shaker connected to the model at the upper flange of the skirt was used to excite the model in a lateral direction. Four piezoelectric accelerometers were mounted on the model, one on each flange and one on top with their axes in line with the direction of excitation, and monitored simultaneously. The model was tested with empty, full, and intermediate liquid conditions and its natural frequencies were recorded. The information so obtained served a dual purpose; it provided data for comparison with the frequencies obtained by an analytical model discussed in the preceding section, and also allowed for the identification of bending modes when the model was later tested in its coupled configuration. This test procedure was also repeated using the Orbiter model.

To determine the natural frequencies of the Booster and Orbiter models along their longitudinal axes, the models were suspended as previously described and excited along their vertical axes by a small electrodynamic shaker. Four piezoelectric accelerometers, mounted on the flanges and the top of the models with their axes along the direction of excitation, were monitored together with pressure transducers installed in the center of each bulkhead. As in the preceding phase, each model was tested with empty, full, and intermediate liquid conditions.

The final step in the test program was the determination of natural frequencies of the complete shuttle vehicle model shown in Fig. 1. The system was suspended in such a manner so that the driving force introduced to the model by the electrodynamic shaker always acted through the gravitational center of the model. Four piezoelectric accelerometers, located on the bottom flanges and the top of the models, were monitored measuring acceleration along the axes of the models, while two others were located at the tops recording acceleration in the lateral direction. In addition, four pressure transducers, one located in each bulkhead, were monitored. All tests were performed with the Orbiter tanks full. The liquid level in the Booster tanks was varied from empty to full with intermediate conditions. Thus, a normal operational sequence was simulated.

Throughout the entire test program, distilled water was used as a modeling liquid propellant. Ullage pressure was provided in all tanks to raise the natural frequencies of nonsymmetric shell modes above the frequency range used during the tests.

As a conclusion to the experimental program, the modeling liquid was replaced in the tanks by a granular substance with bulk density very closely equal to the modeling liquid and the model was

tested at full and half-full levels in the Booster tanks, and similar levels in the Orbiter tanks. This substitution was implemented to facilitate identification of liquid and structural modes in the data obtained from tests completed on the coupled system, as well as to show more vividly the effects of liquid propellants.

Comparison of Results

The output from the theoretical model was in the form of natural frequencies representing:

(1) Rigid body motion of the system (zero frequencies)

(2) Sloshing frequencies of the four liquid-containing tanks

(3) Elastic frequencies of the system.

Regarding the rigid body modes, the analytical model predicts three zero frequencies for the coupled Booster/Orbiter system, and six when the Booster/Orbiter coupling is set to zero. This prediction is consistent with rigid body motion in a plane. The four calculated sloshing frequencies were in the range of 1 to 3 Hz and are quite small when compared with system frequencies. Thus, the sloshing modes are essentially decoupled from the natural frequencies of the total system.

Figures 4, 5, and 6 present a comparison of the theoretically-predicted with the experimentally-determined results. Figure 4 shows the first five frequencies of the Booster alone, and Fig. 5 shows the first three frequencies of the Orbiter alone. The analytical and experimental frequency values are quantitatively compared in Table IV. This agreement index was based upon the maximum (absolute value) percentage error between the theoretical and the experimental values, with the experimental values taken as the basis. The agreement is considered good if this error is within 10%, fair if between 10% and 20%, and poor if greater than 20%.

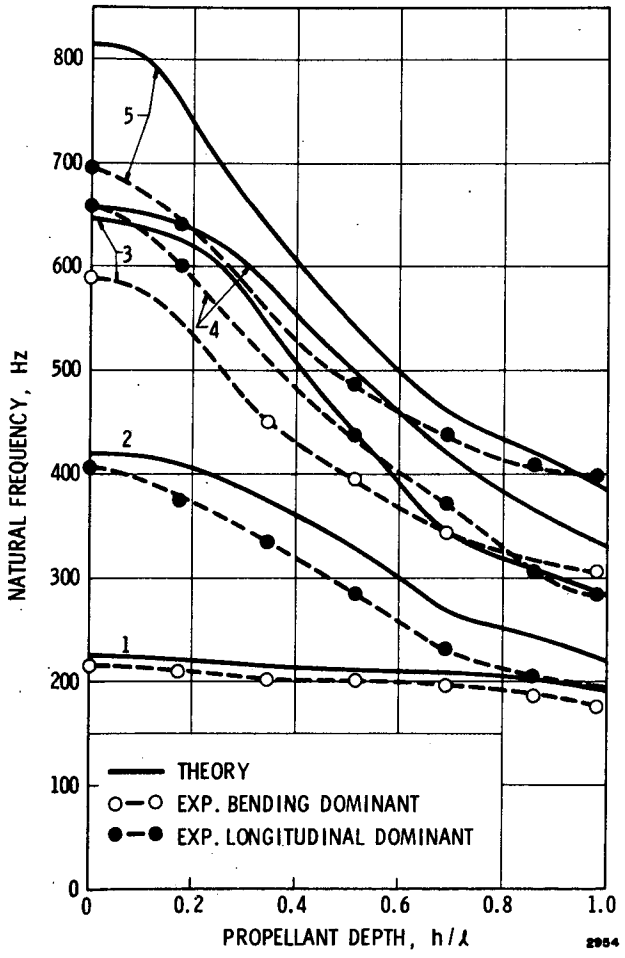

Fig. 4. Uncoupled Booster Natural Frequencies

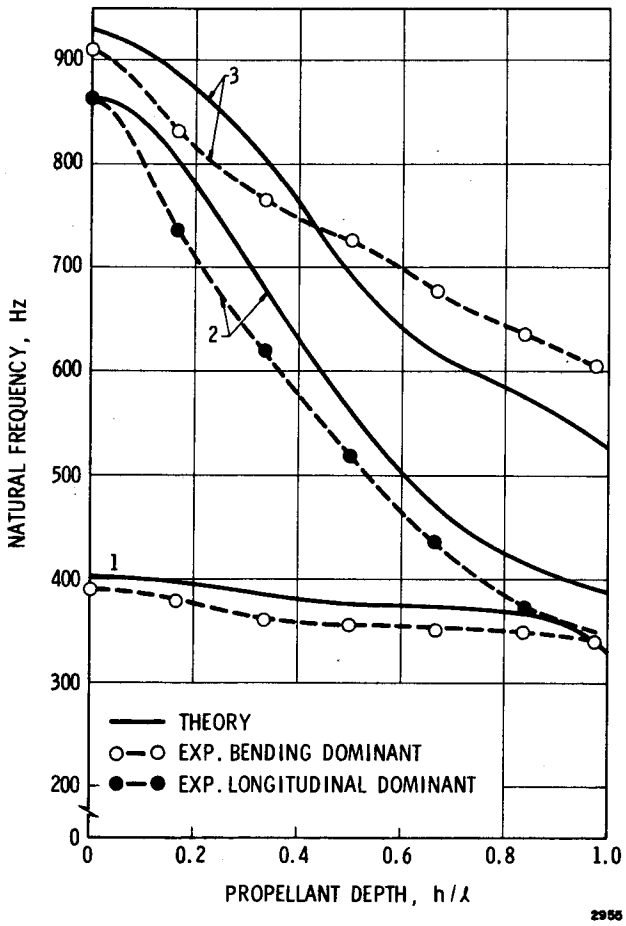

Fig. 5. Uncoupled Orbiter Natural Frequencies

Table IV. Agreement Index for Decoupled Models

BOOSTER

Mode Number	Mode Form	Agreement
1	1st bending	Good
2	1st longitudinal	Fair
3	2nd bending	Good
4	2nd longitudinal	Poor
5	3rd longitudinal	Poor

ORBITER

Mode Number	Mode Form	Agreement
1	1st bending	Good
2	1st longitudinal	Good
3	2nd bending	Good

It is seen from this comparison, and from Figs. 4 and 5, that the agreement between theory and experiment is generally better in the case of bending modes than in the longitudinal modes. There is a particularly significant lack of agreement in the second and third longitudinal Booster modes. Also, the theoretical frequencies tend tc be somewhat higher than the experimental values (except in the case of the second Orbiter bending mode, where the theoretical and experimental curves cross each other).

Table V. A compares the theoretical and experimental frequencies for the coupled empty-tank condition. In terms of the comparison index mentioned above, the agreement is good for the first six modes, and poor for the next three higher modes. It is obvious that above the sixth mode, the relatively simple analytical model is no longer adequate to describe the motion of the system.

Figure 6 compares the theoretical and experimental frequencies for the coupled Booster/Orbiter system for full Orbiter and various Booster propellant levels. The two lowest modes, approximately constant at 15 Hz and 70 Hz, represent modes in which the Booster and Orbiter act essentially as rigid bodies, but vibrate relative to each other through the torsional coupling spring and the lateral coupling spring, respectively. The third mode is dominantly Booster bending, while the fourth mode is the remaining rigid body mode, with relative Booster/Orbiter motion resisted through the longitudinal coupling spring. The fifth and sixth modes exchange motions of dominantly Orbiter bending and Booster longitudinal motion. Above this, the discrepancies become quite large.

Table V. Natural Frequencies for Space Shuttle Vehicle Model

A. All Tanks Empty
(Orbiter Position c = 7.87 in.)

Experimental (Hz)	Theoretical (Hz)		Mode
23.0	23.2	Good	Torsional Coupling
109	105	Good	Lateral Coupling
212	221	Good	Booster Bending
343	355	Good	Longitudinal Coupling
402	417	Good	Orbiter Bending
431	463	Good	Booster-Orbiter Bending
471	649	Poor	
546	659	Poor	
597	815	Poor	
708	863	Poor	

B. Booster and Orbiter $h/\ell = 0.983$ - Granular Propellant
(Orbiter Position c = 7.87 in.)

Experimental (Hz)	Mode
14.7	Torsional Coupling
60.0	Lateral Coupling
436	
845	

C. Booster and Orbiter $h/\ell = 0.517$ - Granular Propellant
(Orbiter Position c = 7.87 in.)

Experimental (Hz)	Mode
14.7	Torsional Coupling
64.0	Lateral Coupling
420	
869	

D. All Tanks Full
(Orbiter Position c = 4.06 in.)

Experimental (Hz)	Mode
15.5	Torsional Coupling
121	Lateral Coupling
171	Booster Bending
191	Booster Longitudinal
216	
300	
310	
416	
458	
476	

E. All Tanks Full
(Orbiter Position c = 11.69 in.)

Experimental (Hz)	Mode
15.2	Torsional Coupling
124	Lateral Coupling
173	Booster Bending
190	Booster Longitudinal
221	
299	
312	

Additional results are shown in Tables V. B and V. C where frequencies are given for the case of a solid-like fluid. A mixture of soil and flour was used to produce a substance having a bulk specific gravity of 1.0. Only the first two modes remained relatively unaltered, while most higher modes disappeared. Apparently, considerably more damping was displayed by this mixture than experienced with water. Thus, in this case a better study of the effects of liquid rather than solid propellant simulation could have been obtained from the analytical model.

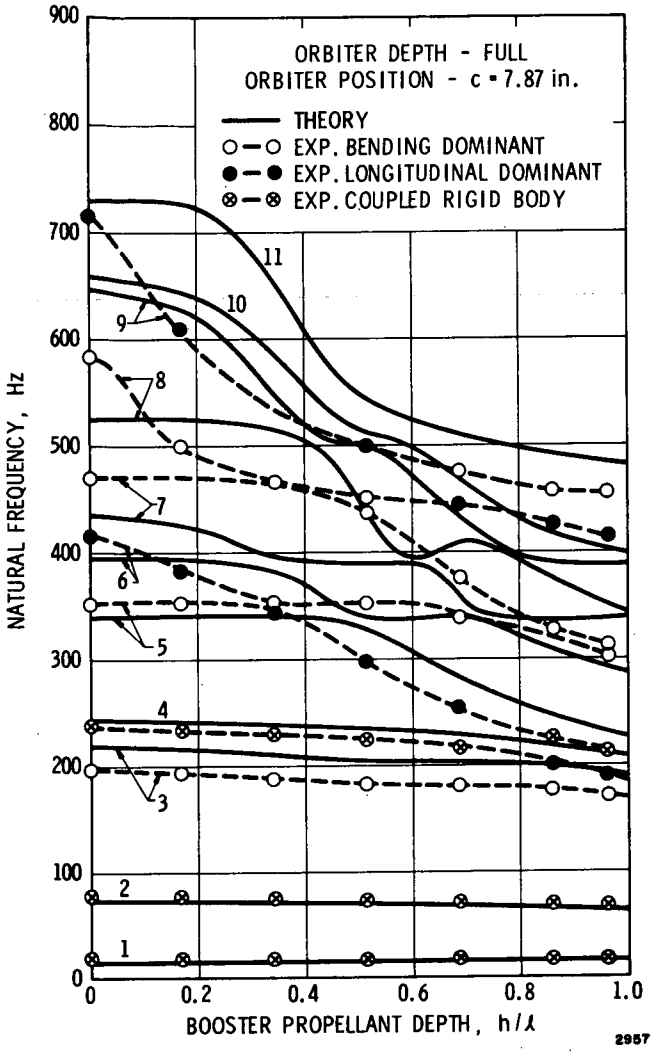

Fig. 6. Natural Frequencies for Space Shuttle Vehicle Model

In Tables V. D and V. E, results are given for alternate positions of the Orbiter on the Booster, when all tanks were full.* In these cases the difference was surprisingly small. Other such results at various liquid levels would be highly desirable.

Finally, Fig. 7 shows an instability that occurs in the system for both Orbiter and Booster full and excitation through the system center of gravity at 453 Hz. The oscilloscope traces show only the pulsating envelope of the high frequency responses. The origin or cause of this type of instability remains to be investigated. However, inspection of the liquid surfaces showed no apparent slosh coupling with the low frequency pulsation, even though it was near the frequency for those modes.

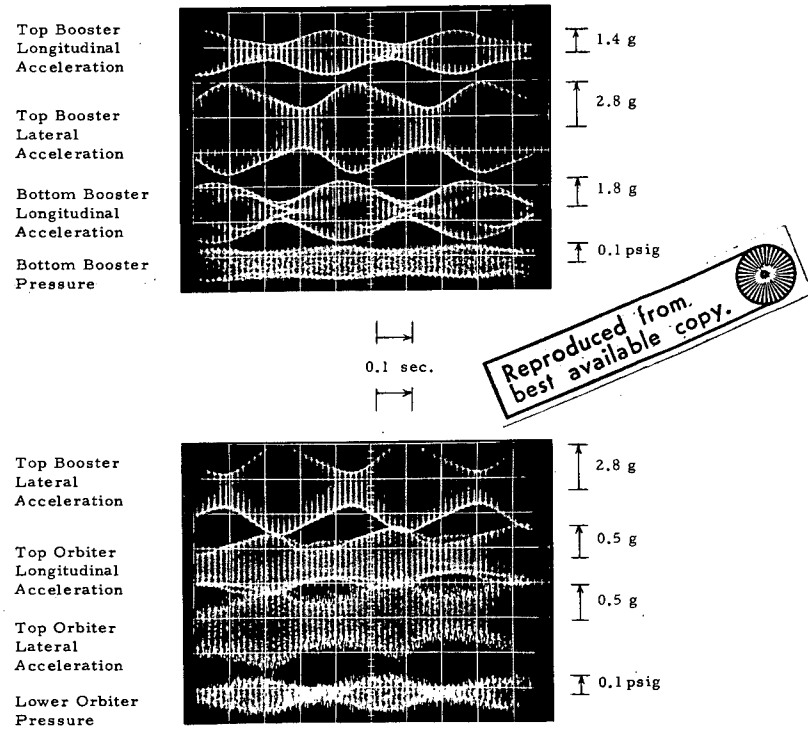

Fig. 7. Space Shuttle Vehicle Model Instability

Conclusions

Experimental and theoretical results of coupled liquid-structural dynamics of a parallel-stage space shuttle vehicle model have been presented. The analytical model developed provides only a fair overall prediction of frequencies for the decoupled Booster and Orbiter models and a somewhat better prediction for the coupled Booster/Orbiter system for the first several modes. One possibility of improving the results at the higher frequencies is to introduce additional modes for the longitudinal liquid sloshing model. Also, a better estimation of joint compliances in the structural model would help.

The results of this study indicate that a very effective, yet rather simple model of a typical space shuttle system has been developed, whereby many potential problems arising in a shuttle vehicle system can be studied.

Acknowledgements

The authors wish to express their sincere appreciation to several individuals who contributed significant efforts toward the conduct of this program. Dr. H. Norman Abramson provided overall consultation, Mr. Luis Garza did

*Because of the coupling design, it was subsequently determined that these results include the effects of the indicated amount of Orbiter position change, as well as effects of an undetermined amount of variation in the coupling springs $K^{(6)}$, $K^{(7)}$, and S_6.

much of the experimental apparatus design, Mr. Herbert G. Pennick performed the computer programming and computations, and Mr. Dennis C. Scheidt and Mr. George W. Downey performed the experiments.

References

1. Proceedings of Space Transportation System Technology Symposium. NASA TM X-52876, Vol. II, Dynamics and Aeroelasticity, NASA Lewis Research Center, July 15-17, 1970.

2. Kana, D. D.; and Nagy, A.: An Experimental Determination of the Longitudinal Modes of a Simulated Launch Vehicle Dynamic Model. Interim Report, Contract No. NAS8-30167, Southwest Research Institute, March 1970.

3. Glaser, R. F.: Longitudinal Mass-Spring Modeling of Launch Vehicles. NASA TN D-5371, 1969.

4. Abramson, H. N.; Chu, W. H.; and Ransleben, G. E.: Representation of Fuel Sloshing in Cylindrical Tanks by an Equivalent Mechanical Model. ARS Journal, pp. 1967-1705, Dec. 1961.

5. Bauer, H. F.: Mechanical Model of Fluid Oscillations in Cylindrical Containers and Introducing of Damping. MTP-AERO-62-16, George C. Marshall Space Flight Center, Huntsville, Alabama, 1962.

6. Abramson, H. N.: The Dynamic Behavior of Liquids in Moving Containers with Applications to Space Vehicle Technology. NASA SP-106, 1966.

7. Pestel, E. C.; and Leckie, F. A.: Matrix Methods in Elastomechanics. McGraw-Hill Book Co., Inc., N. Y., p. 148, 1963.

8. Simmons, J. G.: Modifications of the Timoshenko Beam Equations Necessary for Thin-Walled Circular Tubes. Int. J. Mech. Sci., Vol. 9, pp. 237-244, 1967.

9. Kana, D. D.; Ko, W. L.; Francis, P. H.; and Nagy, A.: Dynamic Interaction Between Structure and Liquid Propellants in a Space Shuttle Vehicle Model. Final Report, Part I, Contract NAS1-9890, Nasa Langley Research Center, October 15, 1971. (NASA CR-111801)